Nano Research

Open Access

Review Article

Grain boundary engineering of metal-based nanomaterials for electrocatalysis

Jie Wang[1,2,§] ✉, Yuecheng Xiong[2,§], Hao Zeng[1], Yishui Tang[1], Weihao Zhong[1], Yuan Shi[1], Dan Wu[1], Fumei Wang[1], Jian Zhou[2], Xichen Zhou[3], and Zhanxi Fan[2] ✉

[1] *Key Laboratory of Fluid and Power Machinery of Ministry of Education, School of Materials Science and Engineering, Xihua University, Chengdu 610039, China*
[2] *Department of Chemistry, City University of Hong Kong, Kowloon, Hong Kong 999077, China*
[3] *Department of Chemistry, The University of Hong Kong, Hong Kong 999077, China*
[§] *Jie Wang and Yuecheng Xiong contributed equally to this work.*

Cite this article: *Nano Research*, **2026**, *19*, 94908534. https://doi.org/10.26599/NR.2026.94908534

ABSTRACT: Grain boundary (GB), as a type of two-dimensional defect in nanocrystals, has recently been identified as a kind of highly active site for various electrocatalytic reactions, such as hydrogen oxidation reaction (HOR), hydrogen evolution reaction (HER), nitrogen/nitrate reduction reaction (NRR/NO_3RR), CO_2 reduction reaction (CO_2RR), oxygen evolution reaction (OER), oxygen reduction reaction (ORR), and alcohol oxidation reaction (methanol/ethanol oxidation reaction (MOR/EOR)). However, there is still a lack of comprehensive reviews examining how GB engineering affects catalytic activity. In this review, we summarize recent advances in GB-engineered metal-based nanomaterials, highlight the remarkable effects of GB, and discuss the structure–performance relationship of GB-rich nanocrystals in electrocatalytic reactions. First, we introduce the synthesis and characterization of GB-engineered nanocatalysts. Next, we thoroughly discuss the relationship between the structure and performance of GB-engineered nanocatalysts. Finally, we outline the challenges and opportunities in this rapidly evolving field, i.e., GB engineering of nanocatalysts.

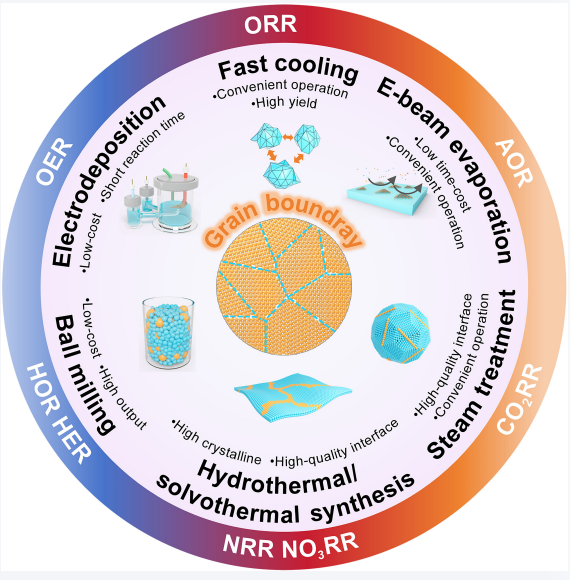

KEYWORDS: metal nanomaterials, grain boundary, electrocatalysis, electrosynthesis, energy conversion

1 Introduction

Grain boundaries (GBs), defined as the interfaces between two crystal grains possessing the same phase but different orientations in a polycrystalline material, have recently been verified as the active sites in a wide range of electrocatalytic reactions. Typically, GBs feature undercoordinated atoms and introduce strain into neighboring grains, resulting in high-energy sites that facilitate the adsorption of reactants and the activation of intermediates in catalytic reactions [1–3]. For example, Kanan's group was among the first to reveal that GBs of metal-based nanocatalysts play an essential role in the electrocatalytic activities in CO_2 reduction reaction (CO_2RR) [4–7]. They found that the surface area-normalized current density for CO_2 reduction to CO (j_{CO}) was linearly correlated with the GB density on the Au electrodes surface at low overpotentials [4]. Also, Huang's group systematically adjusted the GB density in diverse Pt nanostructures and found a positive quadratic correlation between the oxygen reduction reaction (ORR) specific activity and the GB density on the surfaces of the Pt nanostructures [8]. From the previous work, it can be concluded that the active sites available for electrocatalytic reactions will increase by enhancing the GB density or decreasing the grain size, and thus the electrocatalytic performance is expected to be optimized [9, 10].

Furthermore, GB can tailor the local geometrical and electronic

Received: December 30, 2025; **Revised:** February 2, 2026
Accepted: February 3, 2026

✉Address correspondence to Jie Wang, wangjiexhu@mail.xhu.edu.cn; Zhanxi Fan, zhanxi.fan@cityu.edu.hk

environment on catalysts' surface and thus promote the performance of the catalysts [11]. For instance, Hou et al. prepared a GB-rich iridium catalyst (GB-Ir) for hydrogen evolution reaction (HER) [12], and observed that the GB region features a low coordination number, which leads to electron enrichment. This enrichment can promote the water adsorption and lower the energy barrier for water dissociation, leading to the formation of H_3O^+ and creating a localized acid-like chemical environment. This unique environment supplies sufficient protons to facilitate hydrogen spillover from the GB region to more distant areas, thereby enhancing H_2 production [12]. Similarly, in nitrate reduction reaction (NO_3RR), the GB areas in GB-engineered Ni nanocatalysts were found to act as "proton warehouses", which retained the adsorbed H* strongly, suppressing the formation of H_2 and resulting in high NH_3 selectivity [13]. Therefore, GB can regulate the catalytic processes by tuning the local environment on catalyst surfaces.

Taken together, GB engineering of nanomaterials has emerged as an efficient method to optimize the performance of electrocatalysts [10, 11]. However, GB engineering is still in its infancy, and a prompt review is meaningful to contribute to the progress in this promising field (Scheme 1). Herein, a brief discussion about the synthesis and characterization of GB-rich electrocatalysts will be provided first in Section 2. Following that, the electrocatalytic performance of GB-enriched metal nanomaterials in various electrocatalytic reactions including hydrogen oxidation (HOR) and HER, nitrogen reduction reaction (NRR) and NO_3RR, CO_2RR, oxygen evolution and oxygen reduction reaction (OER/ORR), methanol and ethanol oxidation reaction (MOR/EOR) will be summarized in Section 3, highlighting their structure–performance relationships. Lastly, the opportunities and challenges for the development of GB-enriched electrocatalysts will be discussed in Section 4.

2 Synthesis and characterization of GB-enriched nanocatalysts

2.1 Synthesis of GB-enriched nanocatalysts

GB-rich nanomaterials have aroused worldwide interest due to their exceptional performance for electrocatalysis. Although the controlled synthesis of GB-engineered nanomaterials remains challenging, various approaches have been employed to fabricate GB-enriched nanocatalysts, including electrodeposition [13–16], rapid cooling [17, 18], electron beam (E-beam) deposition [4–7], steam treatment [19], hydrothermal/solvothermal synthesis [20], and ball milling [21].

2.1.1 Electrodeposition

Electrochemical methods have been extensively utilized to prepare metal nanoparticles (NPs), since the electrochemical methods can enable the precise control of the synthesis of nanoparticles by fine tuning the applied potential and current density. Thanks to the low cost, easy manipulation, and short reaction time, the electrochemical methods are advantageous to prepare GB-rich nanomaterials. For instance, Zhou et al. proposed the

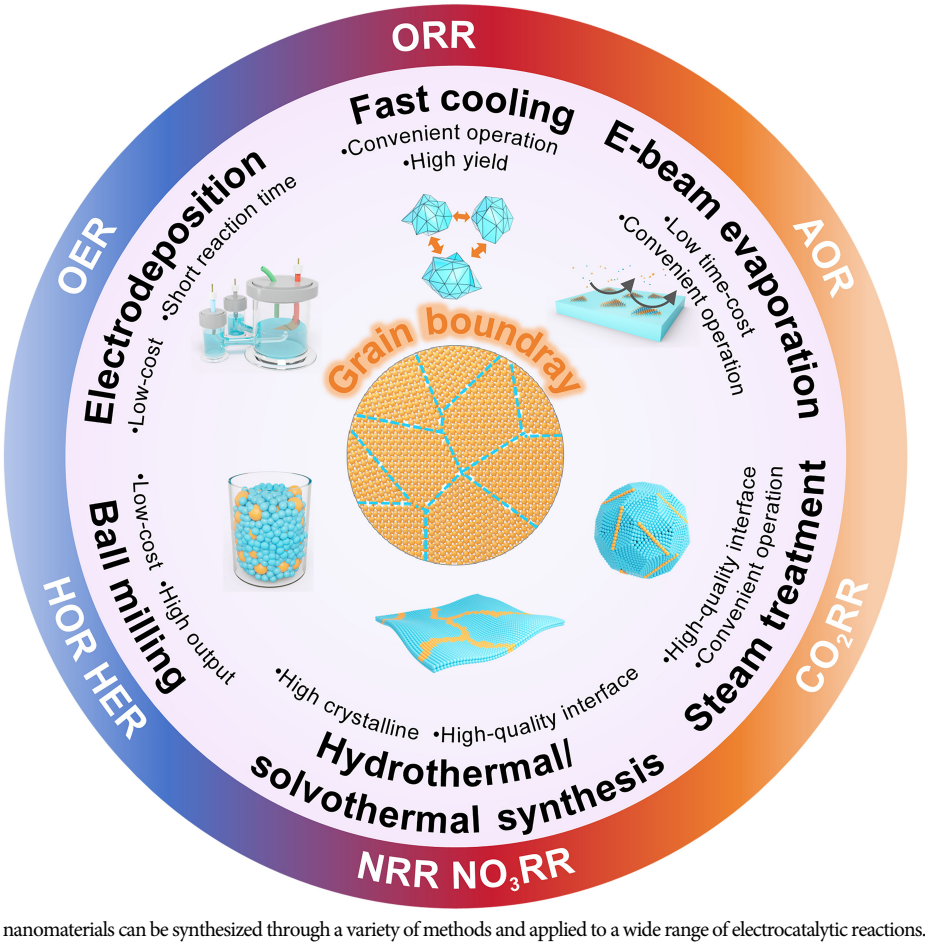

Scheme 1 GB-engineered nanomaterials can be synthesized through a variety of methods and applied to a wide range of electrocatalytic reactions.

electrodeposition method to construct GB-enriched Ni nanoparticles on carbon cloth (Fig. 1(a)). The carbon cloth was applied as the cathode, on which HER and Ni deposition occur and interfere with each other simultaneously, leading to the formation of abundant GB (Figs. 1(b)–1(d)) [13]. In this work, with fixed Ni^{2+} concentration, the applied electrodeposition potential was the key to manipulate the GB density. In another work, Niu et al. prepared Pb-doped Cu nanoparticles via a facile electrodeposition method and the high density of Pb doping was the critical factor for the GB formation [16]. Specifically, they coated carbon paper with a mixture of CuO nanopowders and Pb salts, then employed an *operando* electroreduction process under a CO atmosphere. This process simultaneously reduced the CuO nanoparticles to Cu and enabled the dissolution and redeposition of Pb ions onto the electrode surface. A higher Pb density was observed around the GB area in the Pb-Cu nanocatalysts, revealing that the Pb-doping should be the key factor for the GB formation [16]. Furthermore, the additive utilized in the electrodeposition process can be another important factor. Chen et al. succeeded in fabricating GB-rich Cu nanocatalysts by using poly(vinylpyrrolidone) (PVP) as the additive, which, as an electrochemically inert polymer, can adsorb on Cu surface reversibly and increase the nucleation rate kinetically, resulting in the reduced grain size and thus the enlarged GB density [15]. To conclude, the electrodeposition method is a low-cost but efficient strategy to prepare GB-enriched nanomaterials owing to its facile manipulation and the short reaction-time.

2.1.2 *Fast cooling*

Fast cooling method is another low time-cost strategy in preparing GB-rich nanocatalysts because it can be used to stabilize metastable materials featuring a high density of defects, including GB and dislocations. For example, Du's group used laser ablation in liquid to facilely prepare Ag nanoparticles with a high density of GB [17]. Specifically, the Ag target was first immersed in water, and then the immersed Ag target was heated by a pulsed laser to a plasma state, which was rapidly quenched by cool water to a solid state, and abundant vacancies can be generated and aggregated on the close-packed Ag(111) planes, which can collapse to form GB, during the quenching process (Fig. 2). Nonetheless, water may not be the most effective choice for fast cooling method. For another example, Zheng's group successfully fabricated CuO nanocatalysts with different GB densities by manipulating the quenching rate of the annealed CuO using diverse cooling agents: hot air, water, or liquid nitrogen. In this work, the use of liquid nitrogen, rather than water/hot air, facilitated the fastest cooling process, yielding CuO NPs with the greatest GB density [18]. In brief, fast cooling, as a rapid method, is helpful for the synthesis of GB-rich nanomaterials with convenient operation.

2.1.3 *E-beam evaporation*

As one kind of vapor deposition techniques, E-beam evaporation can enable the formation of precise and uniform thin-film coatings with customized compositions and microstructures by condensing vaporized material onto a substrate, which has been developed as a powerful method to fabricate GB-rich nanomaterials [4–7]. For example, Kanan's group prepared Au/carbon nanotube (CNT) electrodes by using E-beam evaporation to deposit Au atoms on a CNT film [4]. Following that, the Au/CNT samples were annealed under air at different annealing temperatures, which were the key to tune the GB density as annealing at high temperature can facilitate the rise of the grain size and decrease the GB density (Fig. 3) [4]. Similarly, this E-beam evaporation and thermal annealing method can be extended to fabricate GB-rich Cu/CNT electrodes, in which the GB density also declined as the annealing temperature increased [7]. Thus, combining E-beam evaporation (yielding high-density GB) and thermal annealing (decreasing GB density) can not only introduce the high-quality interface but also tune the GB density into the nanomaterials.

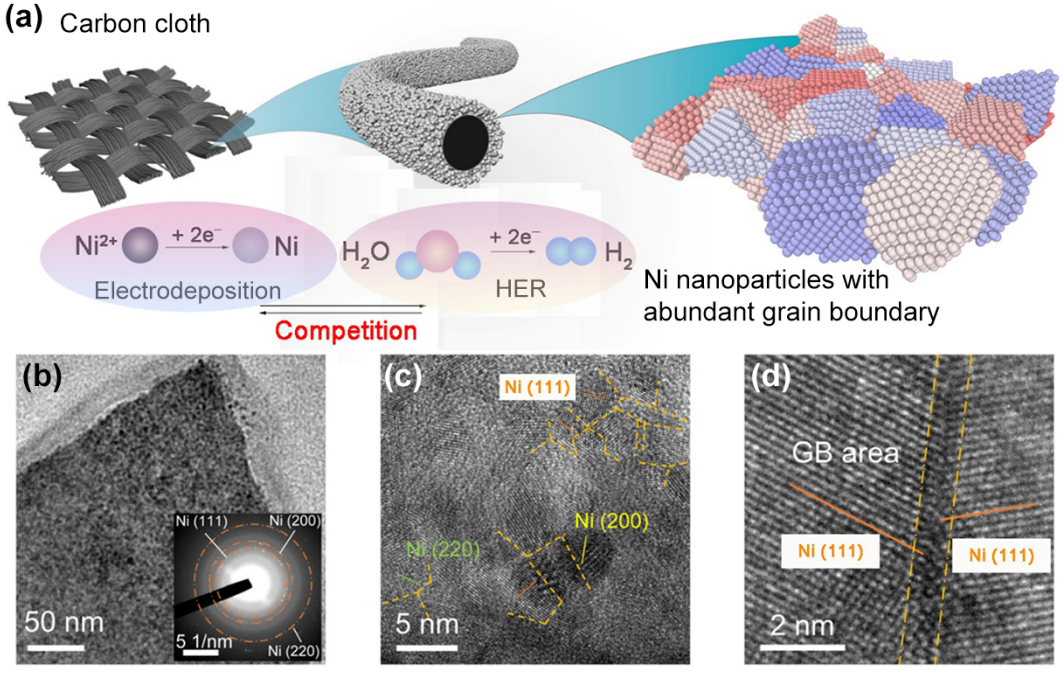

Figure 1 (a) Schematic diagram for the fabrication processes of GB-engineered Ni NPs. (b) TEM image in low magnification with the inset showing the corresponding selected area electron diffraction (SAED) pattern. ((c) and (d)) High-resolution TEM (HRTEM) images of the GB-engineered Ni NPs. Reproduced with permission from Ref. [13], © The Royal Society of Chemistry 2023.

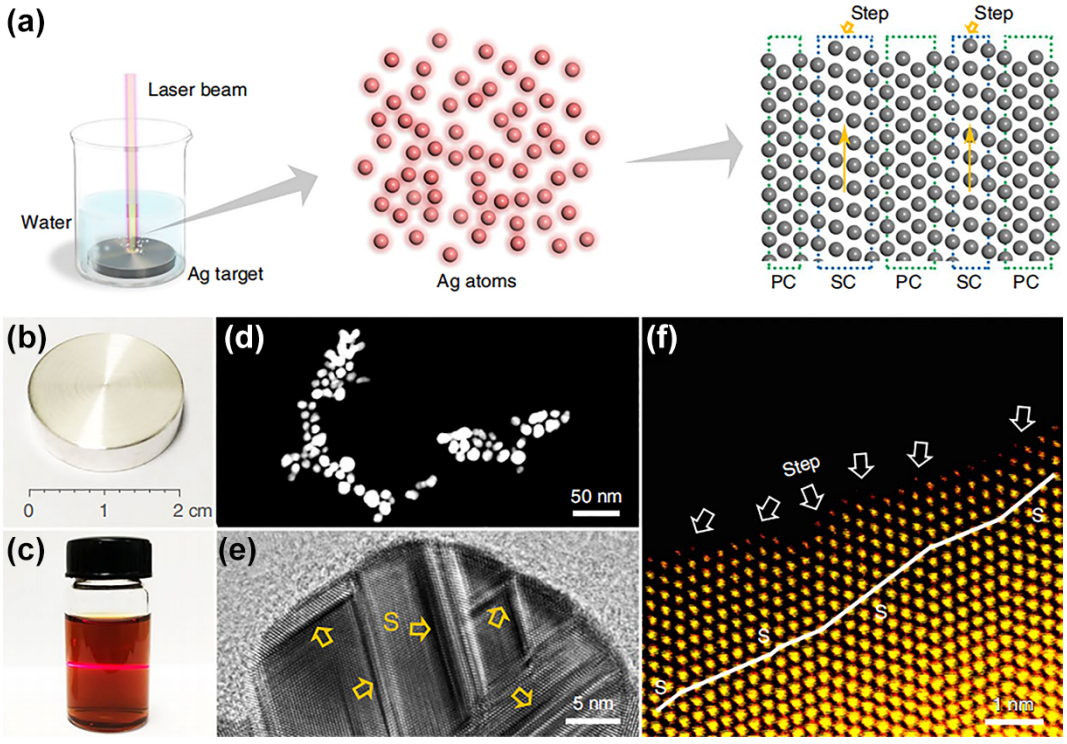

Figure 2 (a) A schematic illustration of the synthesis and structure of laser-generated Ag NP. PC, perfect crystal; SC, stacking fault crystal. ((b) and (c)) Photographs of (b) a silver target and (c) a laser-generated Ag NPs colloidal solution. (d) HAADF-STEM image and (e) HRTEM image of laser-generated Ag NPs. The arrows denote stacking faults. (f) Aberration-corrected HAADF-STEM image of laser-generated Ag NPs. The arrows denote atomic steps. Reproduced with permission from Ref. [17], © Li, Z. et al. 2019.

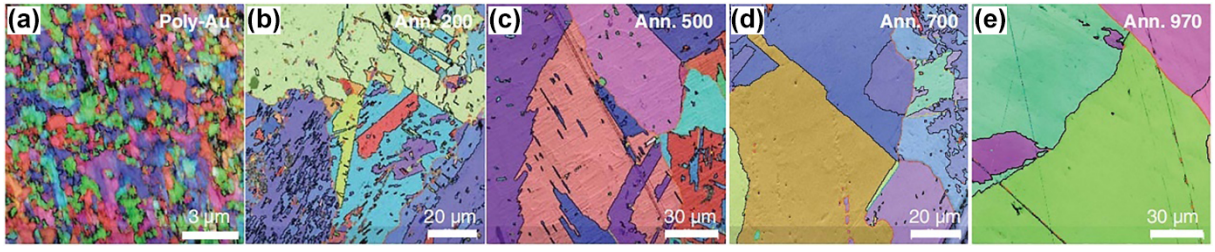

Figure 3 ((a)–(e)) Representative EBSD maps of polycrystalline Au electrodes treated under different annealing temperatures. Each color corresponds to a unique orientation. Reproduced with permission from Ref. [4], © Mariano, R. G. et al. 2017.

2.1.4 *Steam treatment*

Similar to the E-beam deposition methods, the steam treatment can also create high-quality interfaces with simple operation, which is mainly involved in the gas–solid reaction that includes the deposition of new components on the solid precursor by tuning the gas of the tube furnace [19]. Using this method, the atmosphere is generally divided into the reactive gases (e.g., O_2, H_2, PH_3, H_2S, and NH_3) [22–25], which would undergo redox reactions with the solid precursor to yield a different component, and the inert gas (e.g., Ar and N_2), which should facilitate the *in situ* thermal decomposition of the solid precursor (e.g., carbonization) [26–28]. For example, Huang et al. showed that the steam pretreatment of Pd/Al_2O_3 catalyst can result in an increase of the GB density by crystal twinning [19]. Specifically, uniform colloidal Pd nanoparticles were deposited onto a commercial Al_2O_3 support (Pd/Al_2O_3), which was then treated at 600 °C for 0.5 h under H_2O/Ar (4.2/95.8 in volume) (steam-pretreated Pd/Al_2O_3), featuring a GB density of 58 μm^{-1}, much higher than that of Pd/Al_2O_3 (15 μm^{-1}) treated under O_2/Ar, H_2/Ar, or CO/Ar (Fig. 4) [19]. The generation of {111} twin boundaries should be ascribed to the preferential oxidation, which can facilitate the oxygen dissociation and act as the structure precursor to yield GB between the Pd core and the PdO shell. In conclusion, the steam treatment method can bring in high-quality interfaces into the heterostructures with convenient operation.

2.1.5 *Hydrothermal/solvothermal synthesis*

In contrast to the steam treatment method, the hydrothermal/solvothermal method is more favorable for the industrial production of GB-rich nanocatalysts because of its cheap apparatus, simple manipulation, and high product yield [20]. During the hydrothermal/solvothermal synthesis, the precursors are mixed in a harsh environment with high temperature and high pressure, and the chemical composition as well as the morphology of the final product can be controlled by adjusting the input ratio of reactants, solvent, reaction temperature, and time [29]. For instance, Rh ultrathin nanosheets (NSs) with abundant GB are synthesized by a kinetic control approach mediated by CO via the hydrothermal method [20]. Utilizing a mixed solution of formaldehyde and EG, (111)/(110) GB-rich Rh NSs can be generated under a CO-deficient environment (Fig. 5) [20]. In

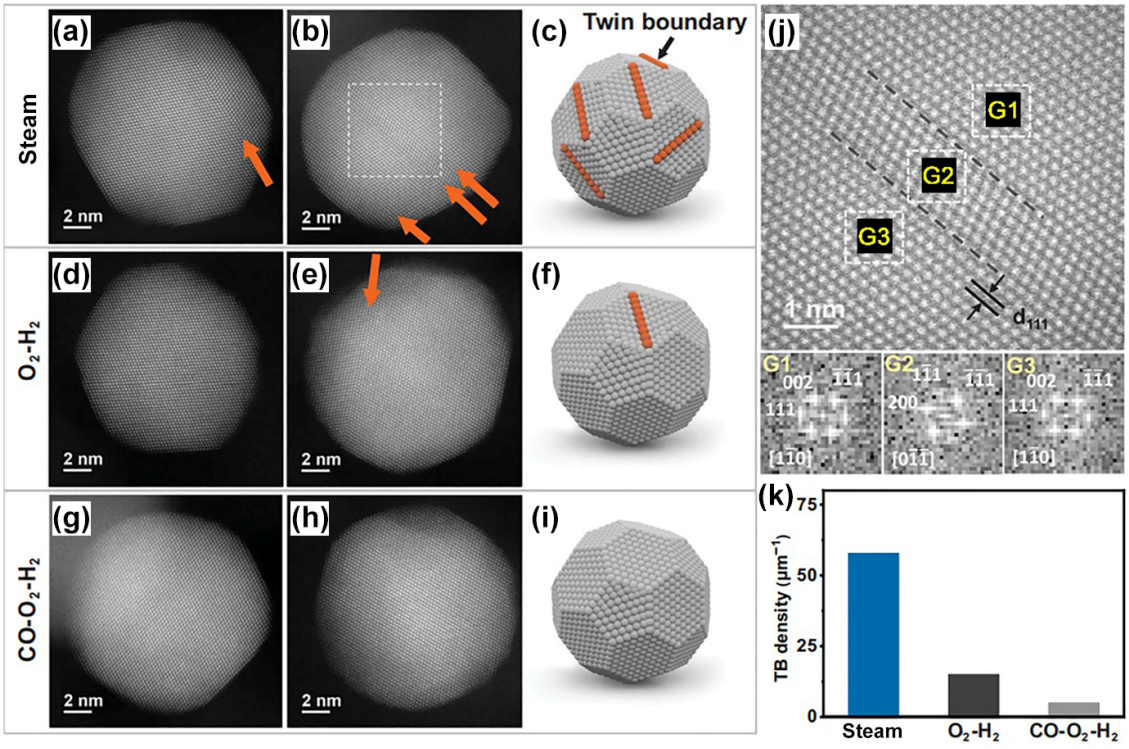

Figure 4 Atomic-resolution HAADF-STEM images of ((a) and (b)) steam-pretreated (600 °C) Pd/Al_2O_3, ((d) and (e)) O_2-H_2-pretreated Pd/Al_2O_3, and ((g) and (h)) CO-O_2-H_2-pretreated Pd/Al_2O_3. ((c), (f), and (i)) Schematic of the twin boundary (TB) density change in Pd NPs after different gas pretreatments. (j) The area marked by the box in (b), revealing the detailed arrangements of Pd atoms. Corresponding fast Fourier transform (FFT) images of grains (G1, G2, and G3) labeled in the top panel. (k) TB density statistical histogram of Pd/Al_2O_3 after steam, O_2-H_2, and CO-O_2-H_2 treatment. Reproduced with permission from Ref. [19], © Huang, W. X. et al. 2021.

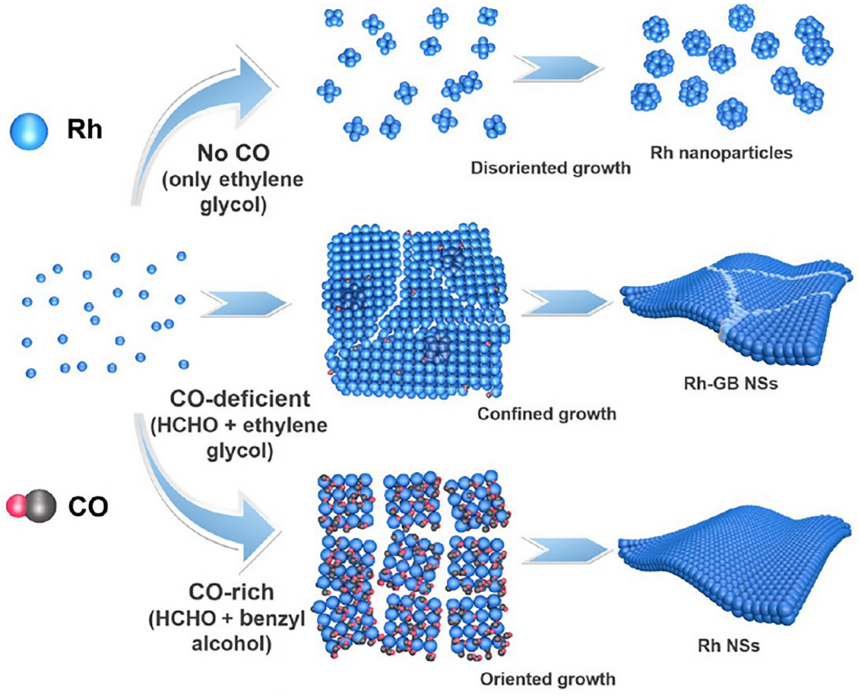

Figure 5 Schematic illustration of the synthesis and structure of Rh nanoparticles, GB-rich Rh NSs, and GB-free Rh NSs. Reproduced with permission from Ref. [20], © American Chemical Society 2023.

addition, Liu and co-workers utilized the hydrothermal method to fabricate ultrathin one-dimensional SnO_2 quantum wires with diameters of less than 2 nm, which were composed of interconnected SnO_2 quantum dots and covered by a high density of GB [30]. Briefly, as a bottom-up approach, the hydrothermal/solvothermal strategy offers a benign and efficient one-pot method for rapidly synthesizing GB-rich nanostructures on a large scale without the need for complex controls.

2.1.6 *Ball milling*

Among all of the above-mentioned synthesis strategies, ball milling is considered as the most efficient one for the industrial preparation of metal-based catalysts, including GB-enriched nanocatalysts, due to its simplicity, efficiency, and economy, which is a mechanical technique and widely employed to grind, mix, or blend bulk materials into nanocomposites [21]. For example, Qiao et al. successfully prepared intermetallic $(Fe_xCo_{1-x})_2B$ (x = 0, 0.33, 0.49, 0.66, 0.83, and 1) electrocatalysts with a controllable GB density by ball milling mixtures of iron powder, cobalt powder, and boron powder at a rotational speed of 900 revolutions per minute (rpm) [21]. The introduction of Fe was critical to give rise to a high density of GB, which can greatly influence the grain size. The small grains were unstable, which should accumulate during the ball milling, and a high density of GB can be generated simultaneously. In brief, ball milling features the advantage of low time-cost and high output in fabricating GB-rich nanocatalysts.

On balance, there have been enormous efforts devoted to developing efficient strategies for preparing GB-rich nanocatalysts (Table 1). Electrodeposition and fast cooling are both low-cost strategies to produce GB, and both E-beam deposition and steam treatment methods can create high-quality interfaces. However, the above four methods suffer from low yield of the product. From the viewpoint of industrial catalytic reactions, apart from the catalytic performance, low energy consumption, simplicity, and high output of the catalysts are also important, indicating that hydrothermal/solvothermal and ball milling methods are more promising for large-scale synthesis of GB-rich electrocatalysts, despite that both of hydrothermal/solvothermal and ball milling methods are low-controllable. Therefore, it is desirable to improve the controllability of hydrothermal/solvothermal and ball milling methods for large-scale synthesis, such as replacing the batch processes by the advanced continuous flow systems, implementing real-time monitoring and automation, and applying systematic scale-up methodologies.

2.2 Characterization of GB-enriched nanocatalysts

GBs are localized defects between material grains, and developing characterization techniques with sufficient resolution for these regions is essential. For example, electron microscopy methods, such as scanning electron microscopy (SEM) and transmission electron microscopy (TEM), are direct analytical tools for studying GB. Notably, electron backscatter diffraction (EBSD) [31], often integrated into SEM systems, provides a non-invasive approach. During the interaction of the electron beam with the sample, backscattered electrons generate individual diffraction patterns. These spatially resolved patterns reveal the crystallographic orientation and misorientation angles of the underlying crystallites, allowing the creation of EBSD orientation maps [4]. These maps visualize the surface grain structure, offering quantitative data on GB density and geometric configurations. Although EBSD can achieve sub-micron resolution for GB visualization, it features limited spatial resolution but stringent sample preparation requirements (e.g., flat, strain-free, and uncontaminated). Thus, EBSD is always integrated with some other analytical techniques (e.g., energy dispersive X-ray spectroscopy (EDS) and *in situ* stages) to provide more comprehensive characterizations.

Furthermore, TEM imaging is indispensable for characterizing nanoscale GB at the atomic level. For instance, Kanan et al. conducted extensive TEM analysis on around 300 Au nanoparticles [5]. They measured the projected GB lengths and particle areas, then used geometric models to convert these values into GB surface lengths and nanoparticle surface areas. By normalizing the total GB surface lengths with respect to the total nanoparticle surface areas, they introduced "GB surface density" as a key metric to evaluate the prevalence of GB (GB density $= \frac{\sum \text{GB surface length of all the counted particles}}{\sum \text{Surface area of all the counted particles}}$) [5]. However, a very limited field of view can be examined by TEM, which might affect the statistical reliability [5]. When combined with aberration correction technology, the analytical capabilities of TEM are greatly enhanced (Fig. 6) [32]. Furthermore, high-angle annular dark field-scanning transmission electron microscopy (HAADF-STEM) imaging of a GB region enables atomic-resolution observations of GB dimensions and chemical composition.

Atom probe tomography (APT) is another advanced technique that provides three-dimensional (3D) chemical mapping of GB with near-atomic resolution [33]. There are growing interests in complementary techniques like Kelvin probe force microscopy (KPFM) [34] for quantitative surface potential mapping and angle-resolved photoelectron spectroscopy (ARPES) [35] for analyzing localized electronic structures. Although conventional methods such as Raman spectroscopy and synchrotron-based X-ray absorption spectroscopy (XAS) have been used to study GB-rich materials [1], they usually require specialized modifications for analyzing the properties of localized GB, whether the analysis is performed *ex situ* or *in situ*. From an electrochemical standpoint, scanning electrochemical cell microscopy (SECCM) offers unique capabilities for imaging electrode processes at the microscale to sub-microscale [36]. This platform allows for the simultaneous acquisition of high-resolution electrochemical activity maps and surface topography. These can be correlated with data from complementary microscopy (e.g., EBSD) or spectroscopy techniques to establish clear relationships between GB structure and activity.

Table 1 A comparison of the synthetic methods for preparing GB-engineered metal-based nanomaterials

Synthetic methods	Electrodeposition	Fast cooling	E-beam evaporation	Steam treatment	Hydrothermal/solvothermal synthesis	Ball milling
GB density control	Good	Good	Excellent	Moderate	Moderate	Moderate
Yield	Moderate	Moderate	Low	Low	High	High
Cost	Low	Low	High	Moderate	Low	Low
Typical materials	Ni, Cu, Pb-Cu alloy nanoparticles, etc.	Ag, CuO nanoparticles, etc.	Au/CNT, Cu/CNT, metal/carbon composite films, etc.	Supported metal catalysts like Pd/Al_2O_3, etc.	Ultrathin Rh nanosheets, SnO_2 quantum wires, etc.	Intermetallic compounds/alloys like $(Fe_xCo_{1-x})_2B$, etc.

清華大學出版社 Tsinghua University Press | SciOpen

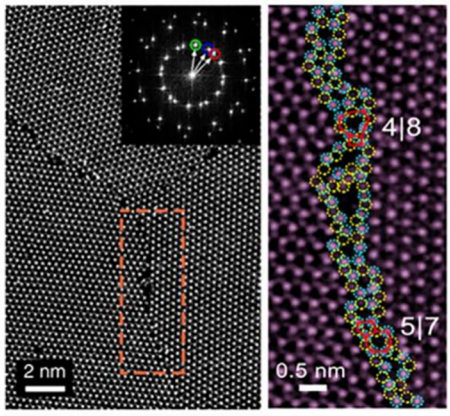

Figure 6 Left panel: HAADF-STEM image showing the GBs between three MoS_2 grains. Inset: FFT of the image showing three distinct sets of MoS_2 diffraction patterns. Right panel: Higher magnification atomic-resolution HAADF-STEM image of the marked region in left, showing the detailed atomic structure of the GBs. Reproduced with permission from Ref. [32], © He, Y. M. et al. 2020.

To conclude, it is necessary to not only take advantage of the characterization techniques with sufficient resolution for atomic-resolution observations of GB-regions, such as EBSD and HAADF-STEM combined with aberration correction, but also develop advanced techniques to analyze the localized electronic structures near GB, including APT, KPFM, and ARPES. Furthermore, SECCM methodology should be highlighted because it enables dynamic electrochemical imaging with remarkable spatial resolution at the microscale to sub-microscale, which is important to establish clear structure–performance relationships of GB.

3 Structure–performance relationship of GB-enriched nanocatalysts in electrocatalysis

In general, the performance of the catalysts is measured by the intrinsic activity, number of active sites, and stability, all of which can be regulated by interfacial engineering through tuning their interfacial microenvironment such as bonding, electronic configuration, lattice strain, and synergistic effects. It is worth noting that the electrocatalytic activity of GB-enriched nanocatalysts is generally influenced by more than one kind of interfacial microenvironment because of the complexity of their structure.

3.1 Hydrogen oxidation reaction/hydrogen evolution reaction

HOR and HER are crucial for hydrogen-based technologies, but the sluggish kinetics of these reactions pose significant challenges [12, 37]. Recent studies have revealed that the incorporation of GB into catalysts can tune the hydrogen binding and enhance the electrocatalytic HOR and HER performance (Fig. 7). To be specific, GBs can provide unsaturated-coordination reactive sites and modulate the binding strength of reaction intermediates. For example, Rh nanosheets with a high density of GB (Rh-GB NSs) showed significantly improved electrocatalytic HOR performance in alkaline solutions, surpassing that of GB-free Rh NSs and the commercial Pt/C catalyst (Fig. 7(d)) [20]. Furthermore, Mondal et al. experimentally found that a flower-like Au nanostructure with a high density of triple-junction GB exhibited much higher HER activities in neutral and acidic media by comparison with other Au nanostructures with fewer GBs, which should be ascribed to the beneficial effect of GB on hydrogen adsorption free energy (ΔG_{H^*}) and the d-band center position based on density functional theory (DFT) calculation [38]. Specifically, when the Au nanostructures change from the GB consisting of three planes ((110), (200), and (111)) to the GB consisting of either of the two planes among (110), (200), and (111), their d-band center shifts toward the Fermi level, leading to the decrease of ΔG_{H^*}, corresponding to the stronger adsorption of hydrogen, and resulting in the decline of HER activity. Thus, this work demonstrates that the GB consisting of three planes ((110), (200), and (111)) has the most favorable d-band center position for moderate H* adsorption, bringing about the improved reaction kinetics toward HER.

Additionally, GBs have also been identified to tailor the local chemical environment on the surface of the catalysts for promoting electrocatalytic reactions. For example, Hou et al. prepared GB-enriched Ir nanostructures and studied their electrocatalytic properties in HER, which exhibited an overpotential of only 10 mV at 10 $mA{\cdot}cm^{-2}$ and a Tafel slope of just 20 $mV{\cdot}dec^{-1}$ in alkaline media [12]. They demonstrated that a local acid-like environment with H_3O^+ intermediates was generated because of the electron-rich surface Ir atoms around GB based on *operando* Raman spectroscopy and DFT calculation results. H_3O^+ intermediates can not only lower the energy barrier for water dissociation, but also provide abundant protons to facilitate the generation of hydrogen spillover from the sites near the GB to the sites far away from the GB, synergistically promoting the HER activity.

Despite the great progress derived from noble metal-based catalysts towards HOR and HER, the development of non-noble metal-based catalysts deserves more attention for making hydrogen technologies more affordable and accessible, such as Cu and transition metal carbides. For instance, although most of Cu nanostructures exhibited poor HER performance because of their weak binding with intermediates, the catalytic activity of pure Cu can be activated by the incorporation of GB. Specifically, Li et al. [1] synthesized GB-rich Cu_2O nanoparticles via pulsed laser ablation and then the Cu_2O particles were electro-reduced to pure Cu, generating distorted nanotwins and edge dislocations (GB-Cu), which can induce high lattice strain and enhance the interaction between Cu and intermediates. As indicated in Figs. 7(a)–7(c), the as-prepared low-cost pure GB-Cu showed superior HER activity and durability to commercial Pt/C catalysts, which featured much lower overpotential (301 mV@50 $mA{\cdot}cm^{-2}$) than that of Pt/C (425 mV@50 $mA{\cdot}cm^{-2}$) [1]. Furthermore, transition metal carbides are also promising candidates for noble metal-based HER/HOR catalysts. For example, Gupta's group synthesized WC nanoparticle films with a high GB density by ion implantation method, which showed favorable intrinsic HER activity and stability (turnover frequency (TOF) = 11 $H_2{\cdot}s^{-1}$, 10 $mA{\cdot}cm^{-2}$ for 12 h) [39]. Also, Zhang's group obtained ultrathin dense polycrystalline Mo_2C nanosheets with rich GB chemically connected to N-doped graphene via Mo–C bond by hydrothermal and water-assisted carbothermal reactions, which afford ultrahigh fraction of active sites for HER and exhibited excellent HER activities (TOF = 21.33 $H_2{\cdot}s^{-1}$ at the overpotential of 100 mV in acidic electrolytes) [40]. In the future, transition metal sulfides and borides should receive more attention, because the hybridization of the d-band structures of transition metals with the orbitals of carbon, sulfur, and boron can modify the free energy of hydrogen adsorption [32, 39–41]. To sum up, the incorporation of GB into nanocatalysts

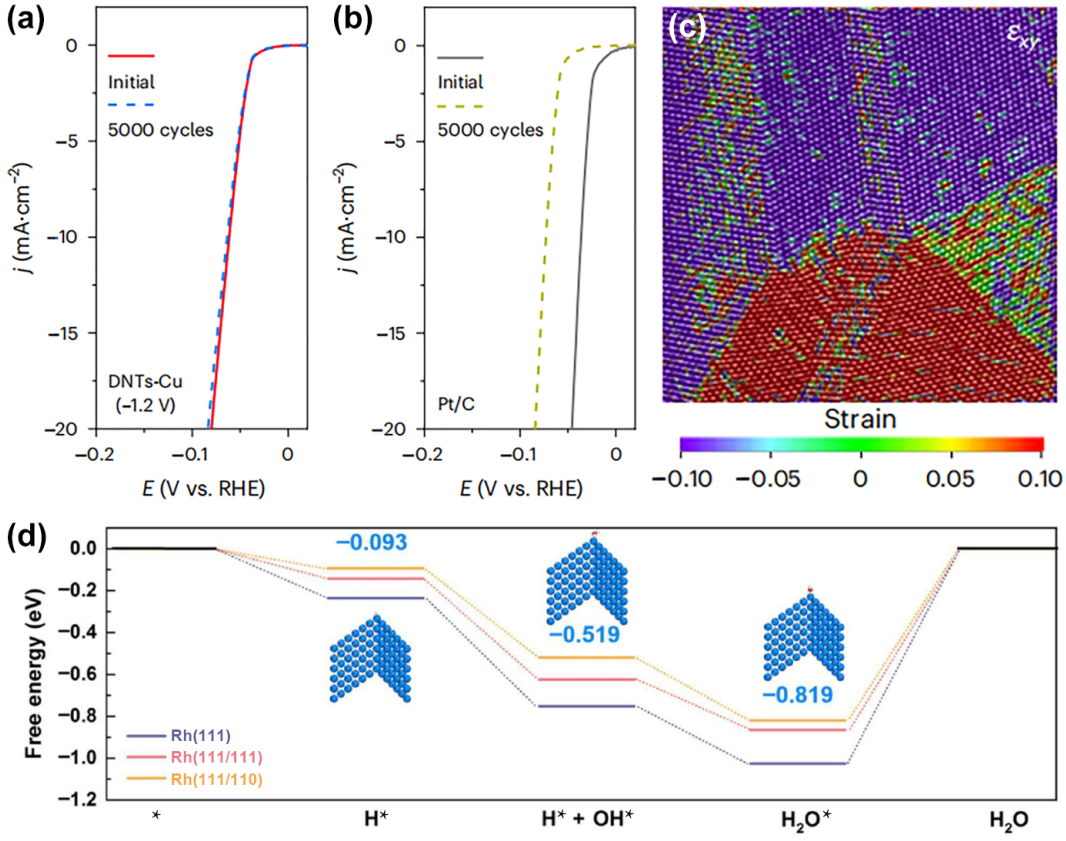

Figure 7 ((a) and (b)) Polarization curves of Cu nanocatalysts with abundant distorted nanotwins (DNTs-Cu) (a and the commercial Pt/C catalysts (b) before and after 5000 cyclic voltammetry (CV) cycles. (c) Geometric phase analysis of the spherical aberration-corrected HRTEM image of the DNTs-Cu (−1.2 V) catalyst. Reproduced with permission from Ref. [1], © Li, Z. et al. 2025. (d) Reaction pathways of Rh(111), Rh(111/111), and Rh(111/110) for the alkaline HOR. Reproduced with permission from Ref. [20], © American Chemical Society 2023.

can promote HER performance by providing more abundant active sites and tuning the hydrogen adsorption free energy.

3.2 Nitrogen and nitrate reduction reactions

Electrocatalytic NRR offers a meaningful method to synthesize ammonia, a practical carbon-free energy carrier, by utilizing renewable electricity, water, and nitrogen as the raw materials [42, 43]. Therefore, great efforts have been devoted in developing highly selective catalysts for NRR with a favorable yield rate. For instance, Zhong et al. developed MoO_2/C catalyst by *in situ* anchoring interfacial intergrown ultrafine MoO_2 nanograins on N-doped carbon fibers [43]. A high density of GB can be yielded between the MoO_2 nanograins by tuning the thermal treatment parameters, which can increase the proportion of oxygen vacancies, facilitate the transfer of electrons, and thereby create highly active reactive sites and efficient nitrogen capture, leading to the outstanding NRR performance (NH_3 yield = 173.7 $\mu g \cdot h^{-1} \cdot mg^{-1}$, Faradaic efficiency (FE) = 27.6%) [43]. *In situ* X-ray photoelectron spectroscopy (XPS) and DFT results confirmed the interaction of N_2 and oxygen vacancy as well as the electronic transfer between N and Mo around GB, demonstrating the great potential of GB-engineering strategy for efficient ammonia production.

Furthermore, the electrocatalytic NO_3RR is another effective avenue for ammonia synthesis under ambient conditions, while highly selective and efficient catalysts are necessary to achieve efficient nitrate-to-ammonia conversion [13, 44–52]. For instance, Zhou et al. electrodeposited Ni nanoparticles on carbon cloth and engineered the GB density by tuning the electrodeposition potential (Fig. 8) [13]. The GB-enriched Ni nanoparticles showed remarkable activity towards nitrate-to-ammonia conversion, achieving an ammonia production rate of 15.49 $mmol \cdot h^{-1} \cdot cm^{-2}$ with FE of 93.0% [13]. Based on DFT results, this outstanding NO_3RR performance should be attributed to the GB sites which can effectively stabilize the H* intermediate, facilitate its transfer to adjacent reaction intermediates in the NO_3RR pathway, and accelerate the rate-limiting step ($NO_3^* \rightarrow NO_2^*$).

3.3 CO_2 reduction reaction

Similar to NRR and NO_3RR, the electrochemical CO_2RR should compete with HER, which is a highly versatile process capable of producing a wide range of valuable chemical products by electricity energy under mild conditions, including C_1 compounds such as CO, CH_4, formic acid, and methanol, and multi-carbon (C_{2+}) products such as C_2H_4, C_2H_6, and ethanol [53–60]. As CO_2RR can not only complete the closure of the artificial carbon cycle, but also realize the synthesis of high-value chemicals, it is meaningful to develop highly-selective and efficient catalysts for CO_2RR from the point of scientific and economic view. Kanan's group conducted a series of seminal work in the development of GB-enriched CO_2RR catalysts, who observed a monotonic increase in j_{CO} of polycrystalline Au electrode with the increase of the total GB density (Figs. 9(a) and 9(b)) [4, 5]. Since then, tremendous efforts have been devoted into engineering GB to obtain more selective and efficient CO_2RR electrocatalysts. For example, Gong's group

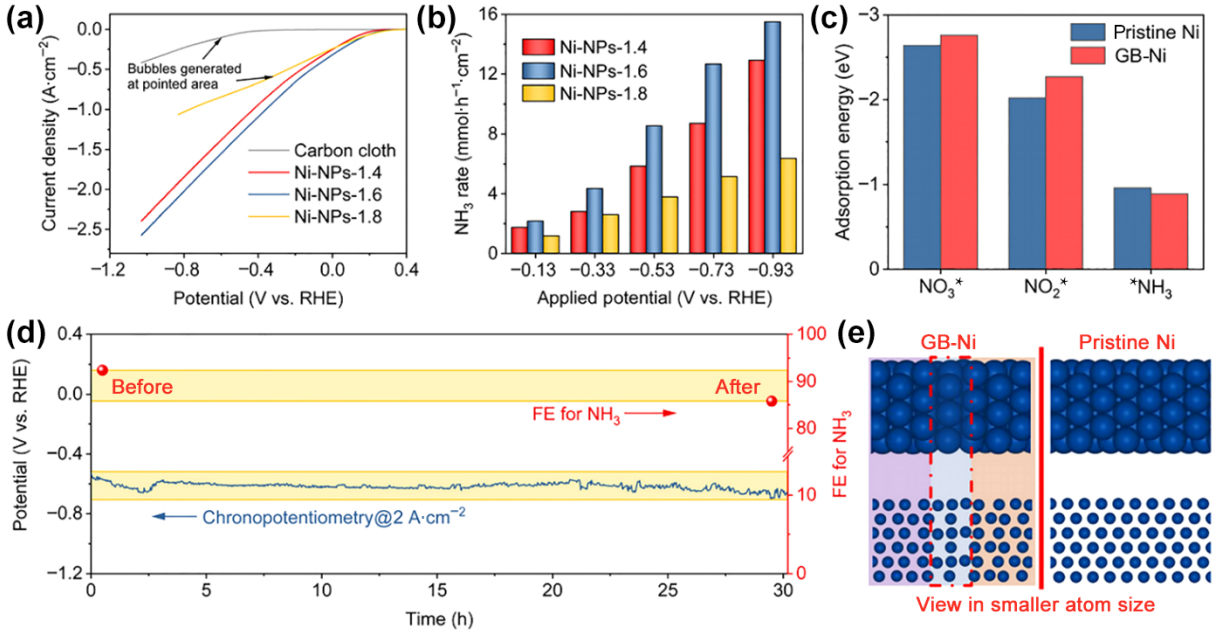

Figure 8 (a) LSV curves of Ni-NPs and carbon cloth for nitrate reduction. (b) Different LSV curves of Ni-NPs. (c) Adsorption energies of H*, NO_3*, and NO_2* on GB-Ni and pristine Ni. (d) Stability test of Ni-NPs-1.6. (e) The built structure model of GB-Ni and pristine Ni for DFT calculations. Reproduced with permission from Ref. [13], © The Royal Society of Chemistry 2023.

derived GB-rich Cu catalysts (GB-Cu) from the electrodeposition method, which featured a much better selectivity (FE = 73%) for C_{2+} products across a wide potential range (−1.0–−1.3 V vs. reversible hydrogen electrode (RHE)) than the Cu catalysts without GB (Figs. 9(c) and 9(d)) [15]. As explained by the DFT results, the introduction of GB to Cu(111) and Cu(100) facets can significantly change the adsorption properties of the key intermediates, promote CO_2 activation, CO protonation, and CO–CHO coupling, and thus facilitate the selectivity for C_{2+} products [15].

In addition, there are growing interests in constructing more complex Cu-based catalysts for CO_2RR. For example, Wu's group investigated the CO_2RR performance of Cu_7Se_4/CuSe nanosheets enriched with GB, which exhibited a high FE of 63.1% towards ethanol [59]. Experimental and theoretical data revealed that GB can tune the local charge distribution and exhibit Cu^+ property, which served as the active sites for CO_2RR [59]. Furthermore, Huang's group conducted an in-depth study on GB engineering in the perovskite oxide La_2CuO_4 for CO_2RR [60]. La_2CuO_4 nanobamboos with rich GB facilitated the production of C_2H_4 (FE = 60%), bulk La_2CuO_4 without distinct GB favored CO production (FE = 91%), and La_2CuO_4 nanorods with intermediate GB yielded a mixture of C_1 and C_2 products without a satisfying selectivity [60]. X-ray absorption spectroscopy (XAS) analysis demonstrated that GB can bring about strain, and then elongate Cu–O and Cu–La bonds, promoting the generation of C_2H_4 [60]. In short, GB can change the electronic structure and the local charge environment of the catalysts, leading to the favorable selectivity and efficiency of CO_2RR.

3.4 Oxygen evolution reaction

For energy conversion technologies, such as the above-mentioned ammonia synthesis, CO_2 reutilization, and water splitting, the anodic reaction, OER, remains the rate-limiting step, whose slow kinetic rate and high overpotential decrease the efficiency of the overall systems [61–63]. Therefore, rational design of OER catalyst is of utmost importance. Recently, GB-engineering strategies in a wide range of transition metal-based composites, such as alloys [14], oxides [64, 65], and hydroxides [66, 67], have been verified to be effective in optimizing the OER activity. For example, Wang et al. prepared Ru nanoparticles with abundant GB (L-Ru) by laser ablation in liquid, which exhibited a much lower overpotential of 202 mV to reach a current density of 10 mA·cm^{-2} than that of the annealed L-Ru (A-Ru) with completely-eliminated GB (284 mV) and the commercial RuO_2 (305 mV) (C-RuO_2) in acidic media (Figs. 10(a) and 10(b)) [68]. They attributed the improved OER performance to the compressive strain around GB based on the extended X-ray absorption fine structure (EXAFS) analysis (Fig. 10(c)) and DFT calculations (Fig. 10(d)) [68]. Additionally, Zhao et al. obtained amorphous-crystalline GB-rich $Cr_{0.53}Ru_{0.47}O_{2-\delta}$ heterostructure NSs and studied their catalytic behaviors in OER, which achieved an extraordinary mass activity of 0.455 A·mg$_{Ru}^{-1}$ at 1.6 V vs. RHE, 5.9-fold higher than that of the commercial RuO_2, and maintained a long-term stability [69]. They demonstrated that the massive GB, Cr–O–Ru interaction, and shortened Ru–O bonds synergistically regulate the adsorption and desorption rates of oxygen intermediates, and account for their outstanding OER performance [69].

3.5 Oxygen reduction reaction

The electrocatalytic ORR is a critical process in fuel cells but its efficiency is largely hindered by sluggish reaction kinetics [70]. GB engineering has been verified as one of the most efficient routes in improving the sluggish reaction kinetics during ORR. For example, Huang's group synthesized Pt nanostructures possessing a large amount of GB, exhibiting superior ORR activity which can be attributed to the increased oxygen residence time around GB sites [8]. Liu et al. synthesized interlaced GB-rich Pd_1Ag_1 nanowires (NWs) via a polyol method, which displayed higher mass activity and half-wave potential than those of the commercial Pt/C and other PdAg counterparts towards ORR (Fig. 11) [71].

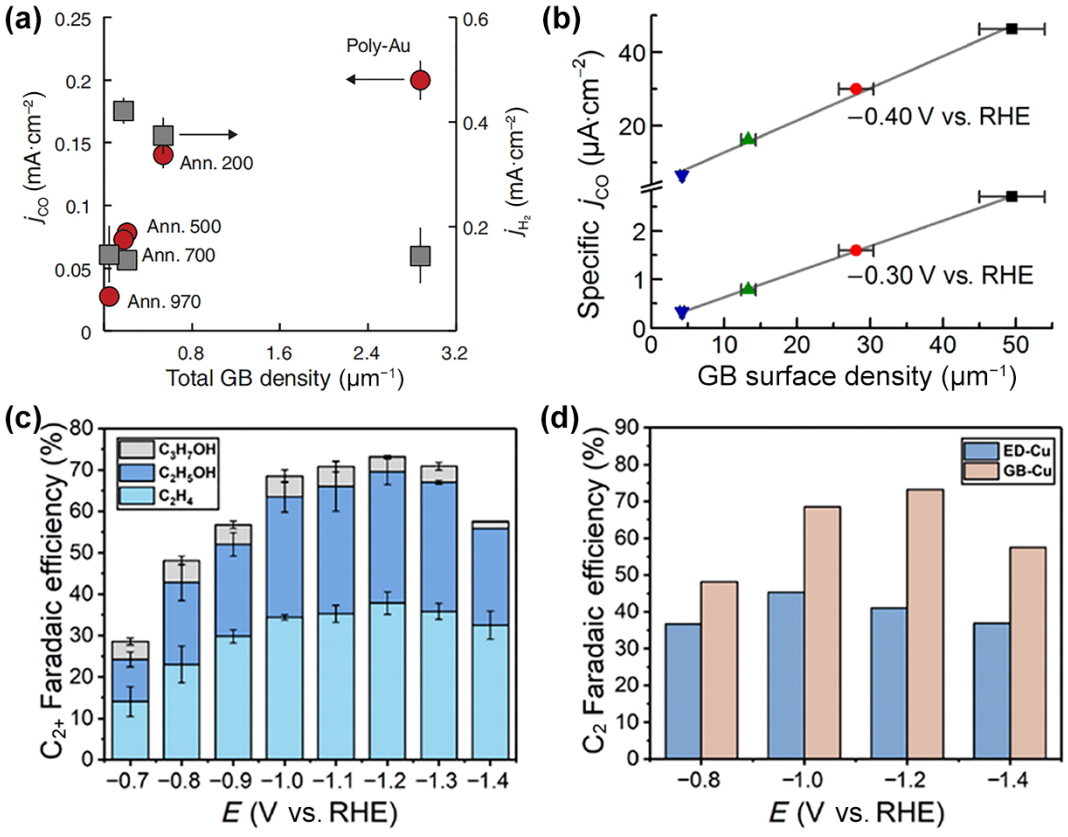

Figure 9 (a) j_{CO} and j_{H_2} versus total GB density for the five Au samples with different densities of GB. Reproduced with permission from Ref. [4], © Mariano, R. G. et al. 2017. (b) Correlation between specific j_{CO} and GB surface density at low overpotentials. Reproduced with permission from Ref. [5], © American Chemical Society 2015. (c) Faradaic efficiencies of C_{2+} products on GB-Cu. (d) Comparison of Faradaic efficiencies of C_2 products on Cu catalysts without GB (ED-Cu) and GB-Cu. Reproduced with permission from Ref. [15], © American Chemical Society 2020.

Therefore, GBs of Pt group-based catalysts have been identified as important active sites for promoting the electrocatalytic ORR activity. Since most of the synthetic methods utilized to tune GB density may change the size, shape, and morphology of the nanostructures at the same time, it is difficult to study the effect of GB on the ORR catalytic performance, such as the activity, selectivity, and stability. To solve these problems, Geng et al. employed Au nanoparticle assemblies (Au-NA) to modify the GB density by manipulating the nanoparticle collision frequency via H_2 bubbling with tunable gas flow rates, and established a proportional relationship between the flow rates, the GB density of Au-NA, and their $2e^-$-ORR activity, that is, the higher the flow rate, the more the high-angle GB, and the better the specific and mass activity (more than two orders of magnitude in contrast to those of the GB-poor Au nanoparticles) [3]. Fourier-transformed X-ray absorption fine structure (EXAFS) spectra confirmed the increased lattice expansion and decreased coordination number as the GB density elevated, both of which jointly resulted in an upward shift in the d-band center and thereby an elevation in the adsorption energy of *OOH on Au based on the theoretical calculation [3]. Furthermore, the durability of the Au-NA with elevated GB density, featuring negligible activity decay over 100 h of operation, was also optimized by comparing with the GB-poor Au nanoparticles, which should be ascribed to the suppressed structural degradation caused by the B segregation around GB. In short, the above-mentioned work provided a potential pathway for constructing advanced ORR electrocatalysts possessing outstanding activity, selectivity, and stability by GB engineering.

3.6 Alcohol oxidation reaction

Substituting OER with the alcohol (e.g., methanol/ethanol) oxidation reactions (AOR) at the anode has been recognized as a promising pathway to lower the energy consumption of emerging technologies (e.g., water electrolyzers, fuel cells, and metal-air batteries) [72–74]. Recent research has already witnessed the success of GB-engineering strategy in maximizing the AOR performance [75–82]. For instance, Huang et al. synthesized Pt nanoworms on graphitic carbon nanosheets (Pt-NWs-CNS) and observed the interconnected Pt nanoworms rich in GBs [78]. As utilized as the MOR catalysts, Pt-NWs-CNS achieved the remarkable mass activity (19.5 A·mg^{-1}), the robust long-term durability, and the superior CO-poisoning resistance. DFT results demonstrated that the worm-like Pt nanostructures rich in GB can modify the electronic structure, accounting for the weakened CO adsorption on Pt surfaces and accelerated reaction kinetics [78].

4 Summary and perspectives

GB, defined as the internal interface between two crystalline grains with different orientations, possesses diverse atomic arrangement in contrast to that of the bulk, and exhibits distinctive physicochemical properties. Specifically, in electrocatalysis, GB could create high-energy surfaces for the adsorption of reactants and activation of intermediates due to the undercoordinated atoms and strain effect around GB sites. Besides, GB can modulate the local environment on the catalysts to promote the performance of GB-enriched

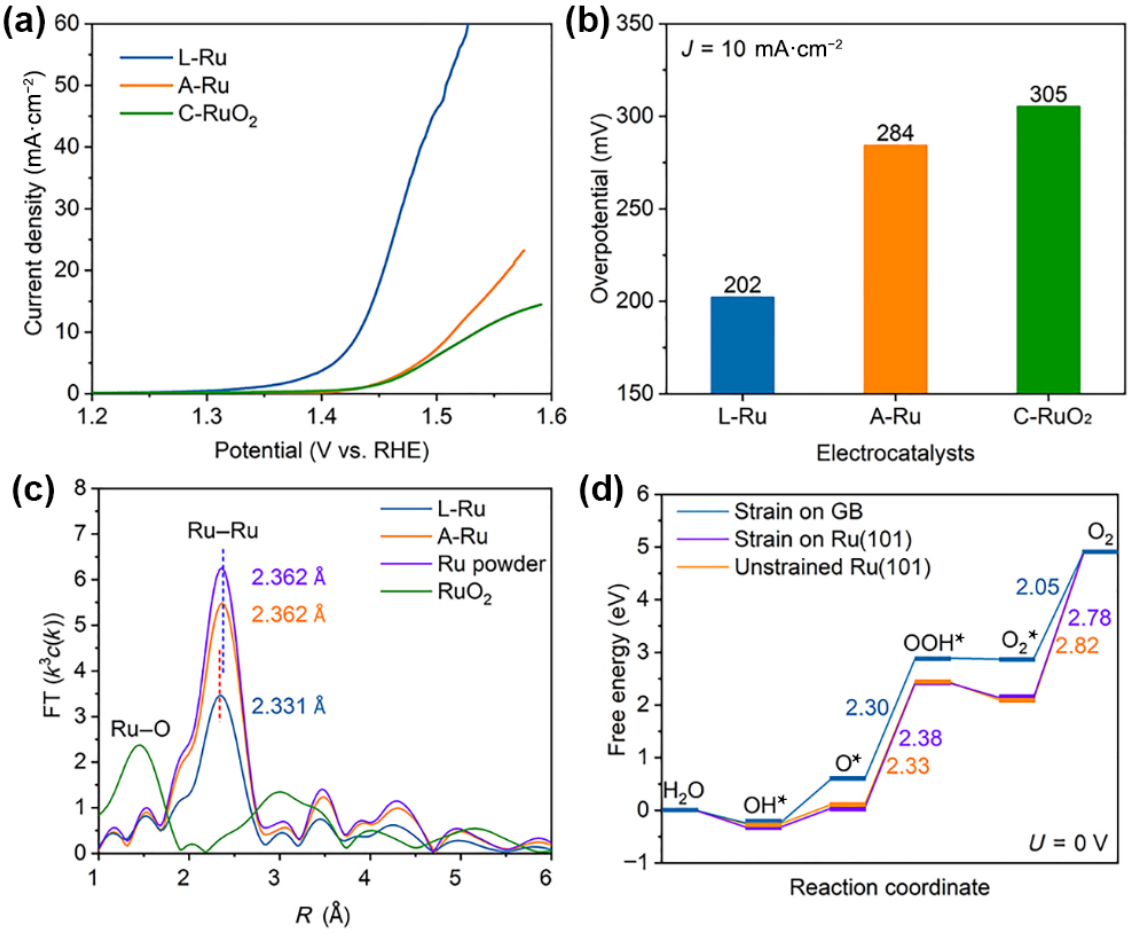

Figure 10 (a) LSV plots of L-Ru, A-Ru, and C-RuO_2 against the corresponding electrochemical active surface area. (b) Overpotentials of L-Ru, A-Ru, and C-RuO_2 at the current density of 10 mA·cm^{-2}. (c) Fourier transform (FT) k^3-weighted EXAFS spectra of L-Ru, A-Ru, metallic Ru powder, and the commercial RuO_2. (d) Free-energy landscape of near Ru(101)-Ru(100) GB with 1.5% compressive strain, strain-free Ru(101) surface, and monocrystal Ru(101) surface with 1.5% compressive strain. Reproduced with permission from Ref. [68], © American Chemical Society 2020.

nanocatalysts. We discussed the synthesis methods, characterization, and applications of GB-engineered nanostructures in HER/HOR, NRR/NO_3RR, CO_2RR, OER, ORR, and AOR. Despite these advances in this fast-developing field, we proposed several research directions deserving future endeavors.

First, for the large-scale industrial application, the scalable synthesis of GB-engineered nanocatalysts of extraordinary current density, robust durability, and especially low cost is indispensable. It is breathtaking to witness that Li's group could prepare GB-enriched Ni-Fe (oxy)hydroxide catalyst on Ni foam through a large-size (10 cm × 10 cm) coating strategy [66], and Luo's group could achieve gram-scale synthesis of GB-rich noble metal nanoparticles assemblies by the electrosynthesis method [83]. It is worth noting that the GB nanostructures should be examined after the further upscaling synthesis. Besides, for the large-scale industrial application, the electrochemical conversion-involved practical devices are generally operated at large current densities, and thus it is necessary for the catalysts to work stably at large current densities (e.g., > 3 A·cm^{-2}). GB-engineered nanostructures have proved to be such a promising candidate for practical applications, while the development of GB-engineered nanostructures is still in its infancy and a huge amount of work should be conducted to explore the influential parameters in GB-engineered nanostructures towards catalysis, such as the composition, density, and angles. Theoretical approaches, including DFT, artificial intelligence (AI), and machine learning (ML), can act as efficient strategies to guide rational design of GB-engineered nanocatalysts, which can rapidly analyze a huge amount of experimental data and provide reasonable guidance about optimal experimental conditions [84–86], in spite of a certain gap between the constructed GB model and the real structures of the as-prepared GB-engineered nanocatalysts. Therefore, the construction of a suitable model to minimize the gap is paramount, which is also conducive to understanding the influential parameters for the optimization of the GB-engineered nanocatalysts and the further upscaling synthesis.

Second, it is highly possible for the active sites of catalysts to reconstruct during the electrocatalytic reactions [87], while GBs, known as high-energy metastable defects, can provide abundant active sites, which might undergo structural relaxations during the harsh electrocatalytic processes. Up to date, *in situ* characterization has been widely utilized to learn the reaction processes of GB-rich catalysts-involved electrocatalysis [12–16], but deficient efforts have been devoted to the dynamic change of GB. For example, by employing the *in situ* electrochemical microscopy, Jang's group observed that oxygen was selectively generated at the GB region [14], but it remains difficult to visualize whether the GB changed or not during OER. The limited progress in the investigation of the dynamic change of GB during electrocatalysis may be ascribed to

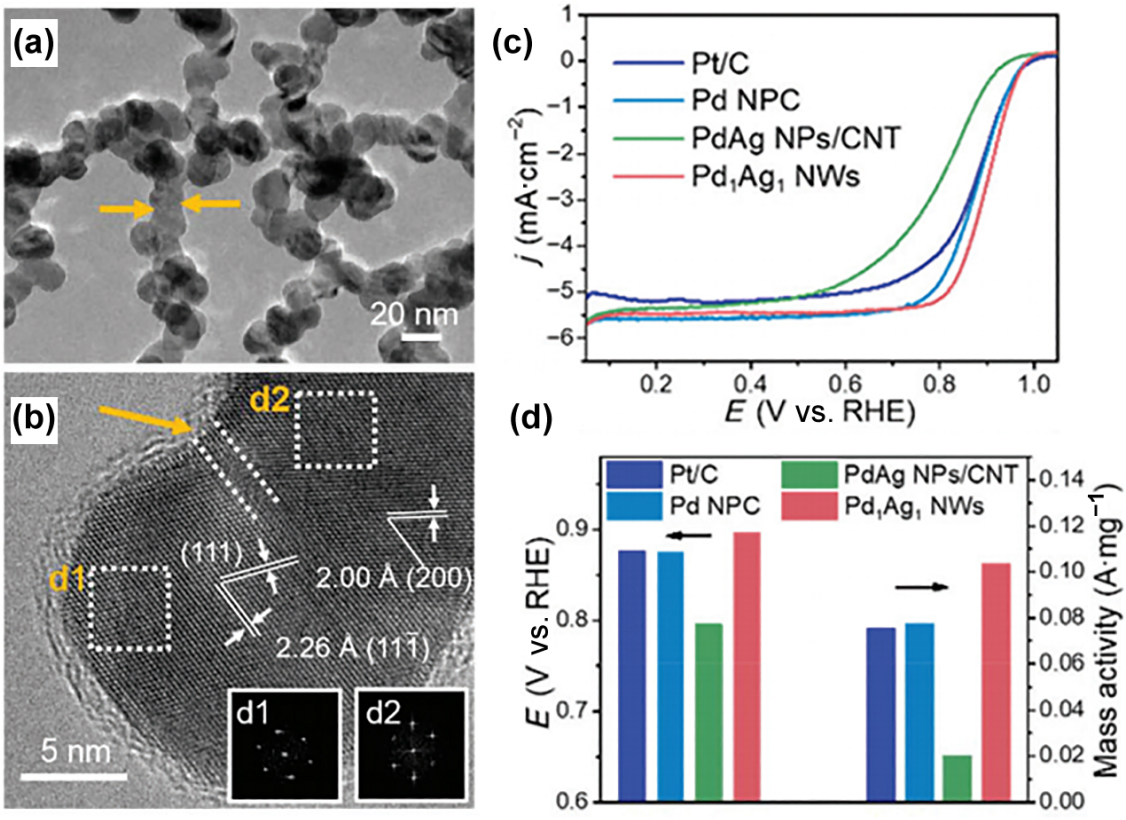

Figure 11 (a) TEM and (b) HRTEM images and the corresponding FFT patterns of the dashed boxes in insets d1 and d2. (c) ORR polarization curves of Pd_1Ag_1 NWs, PdAg NPs, the commercial Pt/C, and the Pd NPC in O_2-saturated 0.1 M KOH. (d) A comparison of the half-wave potentials and mass activities. Reproduced with permission from Ref. [71], © The Royal Society of Chemistry 2020.

the lack of well-established characterization tools capable of locally characterizing the GBs in electrocatalysts. Thus, it is meaningful to take advantage of systematic and advanced *in situ* microscopic-based techniques to study the evolution of the local GB area, such as the size, composition, and structure of the localized GB area, during the electrocatalysis. Last but not least, the development of GB-engineering metal-based nanomaterials can inspire the advancements of other kinds of interfaces in heterostructures, such as phase boundaries (PB) in hetero-phase nanostructures, which, similar with GB, is also able to provide abundant active sites due to the looser atomic arrangement and a large number of defects, including vacancies, dislocations, and deformation. It is exciting to see the successful fabrication of the heterophase noble metal-based Ru_2Ge_3/RuGe intermetallic compounds (IMCs) with engineered PB architecture, which featured outstanding HER performance (overpotential = 135 mV@1000 mA·cm^{-2}) because PB can facilitate charge transfer, promote the kinetics of water dissociation, and optimize the hydrogen adsorption/desorption [88]. However, the manipulation of PB density has rarely been achieved in noble metal-based nanocatalysts and the direct evidence of the relationship between PB and the catalytic performance is still lacking. Thus, PB engineering desires more research attention and more research endeavors should be encouraged in the advancement of PB-engineered nanocatalysts.

In summary, with the combination of theoretical calculations and advanced *in situ* techniques, it is expected to see the burgeoning of GB (or PB)-engineered nanocatalysts in a wide range of catalytic fields such as electrocatalysis and thermocatalysis.

Data availability

Not applicable.

Acknowledgments

This work was financially supported by the Key Project of Sichuan Province (No. 2025YFHZ0225), the Key Project of Liangshan Yi Autonomous Prefecture (No. 23ZDYF0144), the Miaozi Program of Yibin (No. 2025MZ029), and Chengdu Vehicle Environmental Protection Technology Co., Ltd. (No. 2023-CDVEPTKF-04).

Declaration of competing interest

All the contributing authors report no conflict of interests in this work.

Author contribution statement

J. W.: Project administration, funding acquisition, writing manuscript. Y. C. X.: Validation, writing manuscript. H. Z.: writing manuscript, drawing figures. Y. S. T.: writing manuscript, drawing figures. W. H. Z.: writing manuscript, drawing figures. Y. S.: writing manuscript. D. W.: writing manuscript. F. M. W.: writing manuscript. J. Z.: writing manuscript. X. C. Z.: writing manuscrip. Z. X. F.: Project administration, writing manuscript. All the authors have approved the final manuscript.

Use of AI statement

None.

References

[1] Li, Z.; Wang, Y. S.; Liu, H.; Feng, Y.; Du, X. W.; Xie, Z. H.; Zhou, J. H.; Liu, Y.; Song, Y.; Wang, F. et al. Electroreduction-driven distorted nanotwins activate pure Cu for efficient hydrogen evolution. *Nat. Mater.* **2025**, *24*, 424–432.

[2] Yang, Y.; Louisia, S.; Yu, S.; Jin, J. B.; Roh, I.; Chen, C. B.; Fonseca Guzman, M. V.; Feijóo, J.; Chen, P. C.; Wang, H. S. et al. Operando studies reveal active Cu nanograins for CO_2 electroreduction. *Nature* **2023**, *614*, 262–269.

[3] Geng, X.; Vega-Paredes, M.; Wang, Z. Y.; Ophus, C.; Lu, P. F.; Ma, Y.; Zhang, S. Y.; Scheu, C.; Liebscher, C. H.; Gault, B. Grain boundary engineering for efficient and durable electrocatalysis. *Nat. Commun.* **2024**, *15*, 8534.

[4] Mariano, R. G.; McKelvey, K.; White, H. S.; Kanan, M. W. Selective increase in CO_2 electroreduction activity at grain-boundary surface terminations. *Science* **2017**, *358*, 1187–1192.

[5] Feng, X. F.; Jiang, K. L.; Fan, S. S.; Kanan, M. W. Grain-boundary-dependent CO_2 electroreduction activity. *J. Am. Chem. Soc.* **2015**, *137*, 4606–4609.

[6] Li, C. W.; Ciston, J.; Kanan, M. W. Electroreduction of carbon monoxide to liquid fuel on oxide-derived nanocrystalline copper. *Nature* **2014**, *508*, 504–507.

[7] Feng, X. F.; Jiang, K. L.; Fan, S. S.; Kanan, M. W. A direct grain-boundary-activity correlation for CO electroreduction on Cu nanoparticles. *ACS Cent. Sci.* **2016**, *2*, 169–174.

[8] Zhu, E. B.; Xue, W.; Wang, S. Y.; Yan, X. C.; Zhou, J. X.; Liu, Y.; Cai, J.; Liu, E. S.; Jia, Q. Y.; Duan, X. F. et al. Enhancement of oxygen reduction reaction activity by grain boundaries in platinum nanostructures. *Nano Res.* **2020**, *13*, 3310–3314.

[9] Verdaguer-Casadevall, A.; Li, C. W.; Johansson, T. P.; Scott, S. B.; Mckeown, J. T.; Kumar, M.; Stephens, I. E. L.; Kanan, M. W.; Chorkendorff, I. Probing the active surface sites for co reduction on oxide-derived copper electrocatalysts. *J. Am. Chem. Soc.* **2015**, *137*, 9808–9811.

[10] Xu, X. M.; Zhong, Y. J.; Wajrak, M.; Bhatelia, T.; Jiang, S. P.; Shao, Z. P. Grain boundary engineering: An emerging pathway toward efficient electrocatalysis. *InfoMat* **2024**, *6*, e12608.

[11] Liu, F.; Fan, Z. X. Defect engineering of two-dimensional materials for advanced energy conversion and storage. *Chem. Soc. Rev.* **2023**, *52*, 1723–1772.

[12] Hou, L. Q.; Li, Z. J.; Jang, H.; Kim, M. G.; Cho, J.; Liu, S. G.; Liu, X. E. Grain boundary tailors the local chemical environment on iridium surface for alkaline electrocatalytic hydrogen evolution. *Angew. Chem., Int. Ed.* **2024**, *63*, e202315633.

[13] Zhou, J.; Wen, M.; Huang, R.; Wu, Q. S.; Luo, Y. X.; Tian, Y. K.; Wei, G. F.; Fu, Y. Q. Regulating active hydrogen adsorbed on grain boundary defects of nano-nickel for boosting ammonia electrosynthesis from nitrate. *Energy Environ. Sci.* **2023**, *16*, 2611–2620.

[14] Park, H. K.; Ahn, H.; Lee, T. H.; Lee, J. Y.; Lee, M. G.; Lee, S. A.; Yang, J. W.; Kim, S. J.; Ahn, S. H.; Kim, S. Y. et al. Grain boundaries boost oxygen evolution reaction in NiFe electrocatalysts. *Small Methods* **2021**, *5*, 2000755.

[15] Chen, Z. Q.; Wang, T.; Liu, B.; Cheng, D. F.; Hu, C. L.; Zhang, G.; Zhu, W. J.; Wang, H. Y.; Zhao, Z. J.; Gong, J. L. Grain-boundary-rich copper for efficient solar-driven electrochemical CO_2 reduction to ethylene and ethanol. *J. Am. Chem. Soc.* **2020**, *142*, 6878–6883.

[16] Niu, W. Z.; Chen, Z.; Guo, W.; Mao, W.; Liu, Y.; Guo, Y. N.; Chen, J. Z.; Huang, R.; Kang, L.; Ma, Y. W. et al. Pb-rich Cu grain boundary sites for selective CO-to-n-propanol electroconversion. *Nat. Commun.* **2023**, *14*, 4882.

[17] Li, Z.; Fu, J. Y.; Feng, Y.; Dong, C. K.; Liu, H.; Du, X. W. A silver catalyst activated by stacking faults for the hydrogen evolution reaction. *Nat. Catal.* **2019**, *2*, 1107–1114.

[18] Yang, C.; Shen, H. C.; Guan, A. X.; Liu, J. L.; Li, T. F.; Ji, Y. L.; Al-Enizi, A. M.; Zhang, L. J.; Qian, L. P.; Zheng, G. F. Fast cooling induced grain-boundary-rich copper oxide for electrocatalytic carbon dioxide reduction to ethanol. *J. Colloid Interface Sci.* **2020**, *570*, 375–381.

[19] Huang, W. X.; Johnston-Peck, A. C.; Wolter, T.; Yang, W. C.; Xu, L.; Oh, J.; Reeves, B. A.; Zhou, C. S.; Holtz, M.; Herzing, A. A. et al. Steam-created grain boundaries for methane C–H activation in palladium catalysts. *Science* **2021**, *373*, 1518–1523.

[20] Yang, X. D.; Ouyang, B.; Zhao, L.; Shen, Q.; Chen, G. Z.; Sun, Y. Q.; Li, C. C.; Xu, K. Ultrathin Rh nanosheets with rich grain boundaries for efficient hydrogen oxidation electrocatalysis. *J. Am. Chem. Soc.* **2023**, *145*, 27010–27021.

[21] Qiao, X. S.; Kang, H. J.; Li, Y.; Cui, K.; Jia, X.; Wu, X. H.; Qin, W. Grain boundary density and electronic dual modulation of intermetallic Co_2B by Fe doping toward efficient catalyst for oxygen evolution reaction. *Appl. Catal. B.* **2022**, *305*, 121034.

[22] Su, L. X.; Gong, D.; Yao, N.; Li, Y. B.; Li, Z.; Luo, W. Modification of the intermediate binding energies on Ni/Ni_3N heterostructure for enhanced alkaline hydrogen oxidation reaction. *Adv. Funct. Mater.* **2021**, *31*, 2106156.

[23] Liu, Y. P.; Yu, G. T.; Li, G. D.; Sun, Y. H.; Asefa, T.; Chen, W.; Zou, X. X. Coupling Mo_2C with nitrogen-rich nanocarbon leads to efficient hydrogen-evolution electrocatalytic sites. *Angew. Chem., Int. Ed.* **2015**, *127*, 10902–10907.

[24] Wu, J.; Zhong, W. D.; Yang, C. F.; Xu, W. L.; Zhao, R.; Xiang, H.; Zhang, Q.; Li, X. K.; Yang, N. J. Sulfur-vacancy rich nonstoichiometric TiS_{2-x}/NiS heterostructures for superior universal hydrogen evolution. *Appl. Catal. B* **2022**, *310*, 121332.

[25] Ma, F. H.; Wang, S. H.; Gong, X. Q.; Liu, X. L.; Wang, Z. Y.; Wang, P.; Liu, Y. Y.; Cheng, H. F.; Dai, Y.; Zheng, Z. K. et al. Highly efficient electrocatalytic hydrogen evolution coupled with upcycling of microplastics in seawater enabled via Ni_3N/W_5N_4 janus nanostructures. *Appl. Catal. B* **2022**, *307*, 121198.

[26] Wang, P. Y.; Zhu, J. W.; Pu, Z. H.; Qin, R.; Zhang, C. T.; Chen, D.; Liu, Q.; Wu, D. L.; Li, W. Q.; Liu, S. L. et al. Interfacial engineering of Co nanoparticles/Co_2C nanowires boosts overall water splitting kinetics. *Appl. Catal. B* **2021**, *296*, 120334.

[27] Fang, Y.; Xue, Y. R.; Li, Y. J.; Yu, H. D.; Hui, L.; Liu, Y. X.; Xing, C. Y.; Zhang, C.; Zhang, D. Y.; Wang, Z. Q. et al. Graphdiyne interface engineering: Highly active and selective ammonia synthesis. *Angew. Chem., Int. Ed.* **2020**, *59*, 13021–13027.

[28] Li, Y. B.; Tan, X.; Tan, H.; Ren, H. J.; Chen, S.; Yang, W. F.; Smith, S. C.; Zhao, C. Phosphine vapor-assisted construction of heterostructured $Ni_2P/NiTe_2$ catalysts for efficient hydrogen evolution. *Energy Environ. Sci.* **2020**, *13*, 1799–1807.

[29] Wang, Y. H.; Xiong, Y. C.; Sun, M. Z.; Zhou, J. W.; Hao, F. K.; Zhang, Q. H.; Ye, C. L.; Wang, X. X.; Xu, Z. H.; Wa, Q. B. et al. Controlled synthesis of unconventional phase alloy nanobranches for highly selective electrocatalytic nitrite reduction to ammonia. *Angew. Chem., Int. Ed.* **2024**, *63*, e202402841.

[30] Liu, S. B.; Xiao, J.; Lu, X. F.; Wang, J.; Wang, X.; Lou, X. W. Efficient electrochemical reduction of CO_2 to HCOOH over sub-2 nm SnO_2 quantum wires with exposed grain boundaries. *Angew. Chem., Int. Ed.* **2019**, *58*, 8499–8503.

[31] Humphreys, F. J. Review grain and subgrain characterisation by electron backscatter diffraction. *J. Mater. Sci.* **2001**, *36*, 3833–3854.

[32] He, Y. M.; Tang, P. Y.; Hu, Z. L.; He, Q. Y.; Zhu, C.; Wang, L.Q.; Zeng, Q. S.; Golani, P.; Gao, G. H.; Fu, W. et al. Engineering grain boundaries at the 2D limit for the hydrogen evolution reaction. *Nat. Commun.* **2020**, *11*, 57.

[33] Luo, T.; Kuo, J. J.; Griffith, K. J.; Imasato, K.; Cojocaru-Mirédin, O.; Wuttig, M.; Baptiste, G.; Yuan, Y.; Snyder, G. J. Nb-mediated grain growth and grain-boundary engineering in Mg_3Sb_2-based thermoelectric materials. *Adv. Funct. Mater.* **2021**, *31*, 2100258.

[34] Nicoara, N.; Manaligod, R.; Jackson, P.; Hariskos, D.; Witte, W.; Sozzi, G.; Menozzi, R.; Sadewasser, S. Direct evidence for grain

boundary passivation in Cu(In,Ga)Se_2 solar cells through alkali-fluoride post-deposition treatments. *Nat. Commun.* **2019**, *10*, 3980.

[35] Ma, Y. J.; Diaz, H. C.; Avila, J.; Chen, C. Y.; Kalappattil, V.; Das, R.; Phan, M. H.; Čadež, T.; Carmelo, J. M. P.; Asensio, M. C. et al. Angle resolved photoemission spectroscopy reveals spin charge separation in metallic $MoSe_2$ grain boundary. *Nat. Commun.* **2017**, *8*, 14231.

[36] Daviddi, E.; Gaudin, L. F.; Bentley, C. L. Scanning electrochemical cell microscopy: High-resolution structure–property studies of mono- and polycrystalline electrode materials. *Curr. Opin. Electrochem.* **2022**, *34*, 101006.

[37] Fan, Z. X.; Luo, Z. M.; Huang, X.; Li, B.; Chen, Y.; Wang, J.; Hu, Y. L.; Zhang, H. Synthesis of 4H/fcc noble multimetallic nanoribbons for electrocatalytic hydrogen evolution reaction. *J. Am. Chem. Soc.* **2016**, *138*, 1414–1419.

[38] Mondal, S.; De, S. K.; Jana, R.; Roy, A.; Mukherjee, M.; Datta, A.; Satpati, B.; Senapati, D. Unveiling the excellent electrocatalytic activity of grain-boundary enriched anisotropic pure gold nanostructures toward hydrogen evolution reaction: A combined approach of experiment and theory. *ACS Appl. Energy Mater.* **2021**, *4*, 3017–3032.

[39] Malone, N.; Fiedler, H.; Mitchell, D. R. G.; Kennedy, J. V.; Waterhouse, G.; Gupta, P. Grain boundary-rich tungsten carbide nanoparticle films exhibit high intrinsic activity toward hydrogen evolution. *ACS Appl. Nano Mater.* **2024**, *7*, 4843–4852.

[40] Yang, Y.; Qian, Y. M.; Luo, Z. P.; Li, H. J.; Chen, L. L.; Cao, X. M.; Wei, S. Q.; Zhou, B.; Zhang, Z. H.; Chen, S. et al. Water induced ultrathin Mo_2C nanosheets with high-density grain boundaries for enhanced hydrogen evolution. *Nat. Commun.* **2022**, *13*, 7225.

[41] Shen, J.; Aljarb, A.; Cai, Y. C.; Liu, X.; Min, J. C.; Wang, Y. G.; Wang, Q. X.; Zhang, C. H.; Chen, C. L.; Hakami, M. et al. Engineering grain boundaries in monolayer molybdenum disulfide for efficient water-ion separation. *Science* **2025**, *387*, 776–782.

[42] Suryanto, B. H. R.; Matuszek, K.; Choi, J.; Hodgetts, R. Y.; Du, H. L.; Bakker, J. M.; Kang, C. S. M.; Cherepanov, P. V.; Simonov, A. N.; MacFarlane, D. R. Nitrogen reduction to ammonia at high efficiency and rates based on a phosphonium proton shuttle. *Science* **2021**, *372*, 1187–1191.

[43] Zhong, X.; Yuan, E. X.; Yang, F.; Liu, Y.; Lu, H.; Yang, J.; Gao, F.; Zhou, Y.; Pan, J. M.; Zhu, J. W. et al. Optimizing oxygen vacancies through grain boundary engineering to enhance electrocatalytic nitrogen reduction. *Proc. Natl. Acad. Sci. USA* **2023**, *120*, e2306673120.

[44] Wang, Y. H.; Sun, M. Z.; Zhou, J. W.; Xiong, Y. C.; Zhang, Q. H.; Ye, C. L.; Wang, X. X.; Lu, P. Y.; Feng, T. Y.; Hao, F. K. et al. Atomic coordination environment engineering of bimetallic alloy nanostructures for efficient ammonia electrosynthesis from nitrate. *Proc. Natl. Acad. Sci. USA* **2023**, *120*, e2306461120.

[45] Ma, Y. B.; Guo, L.; Chang, L.; Guo, W. H.; Zhou, T.; Hao, F. K.; Su, W. D.; Zhou, J. W.; Wang, G. Z.; Shao, M. Z. et al. Unconventional phase metal heteronanostructures with tunable exposed interface for efficient tandem nitrate electroreduction to ammonia. *Nat. Commun.* **2025**, *16*, 7632.

[46] Zhou, J. W.; Liu, F.; Xu, Z. H.; Yin, J. A.; Guo, L.; Hao, F. K.; Wang, Y. H.; Xiong, Y. C.; Zhou, X. C.; Wang, C. et al. Modulating the nitrate reduction pathway on unconventional phase ultrathin nanoalloys for selective ammonia electrosynthesis. *J. Am. Chem. Soc.* **2025**, *147*, 23226–23238.

[47] Wang, Y. H.; Hao, F. K.; Xu, H. M.; Sun, M. Z.; Wang, X. X.; Xiong, Y. C.; Zhou, J. W.; Liu, F.; Hu, Y. B.; Ma, Y. B. et al. Interfacial water structure modulation on unconventional phase non-precious metal alloy nanostructures for efficient nitrate electroreduction to ammonia in neutral media. *Angew. Chem., Int. Ed.* **2025**, *64*, e202508617.

[48] Liu, F.; Zhou, J. W.; Sun, M. Z.; Xu, Z. H.; Wang, H. L.; Yao, N.; Wang, Y. H.; Hao, F. K.; Xiong, Y. C.; Wang, J. et al. Enhanced p-d orbital coupling in unconventional phase RhSb alloy nanoflowers for efficient ammonia electrosynthesis in neutral media. *Angew. Chem., Int. Ed.* **2025**, *64*, e202504641.

[49] Wang, Y. H.; Hao, F. K.; Sun, M. Z.; Liu, M. T.; Zhou, J. W.; Xiong, Y. C.; Ye, C. L.; Wang, X. X.; Liu, F.; Wang, J. et al. Crystal phase engineering of ultrathin alloy nanostructures for highly efficient electroreduction of nitrate to ammonia. *Adv. Mater.* **2024**, *36*, 2313548.

[50] Xiong, Y. C.; Wang, Y. H.; Sun, M. Z.; Chen, J.; Zhou, J. W.; Hao, F. K.; Liu, F.; Lu, P. Y.; Meng, X.; Guo, L. et al. Regulating the electrochemical nitrate reduction performance with controllable distribution of unconventional phase copper on alloy nanostructures. *Adv. Mater.* **2024**, *36*, 2407889.

[51] Xiong, Y. C.; Wang, Y. H.; Zhou, J. W.; Liu, F.; Hao, F. K.; Fan, Z. X. Electrochemical nitrate reduction: Ammonia synthesis and the beyond. *Adv. Mater.* **2024**, *36*, 2304021.

[52] Wang, Y.; Xia, S.; Cai, R.; Zhang, J. F.; Wang, J. R.; Yu, C. P.; Cui, J. W.; Zhang, Y.; Wu, J. J.; Yang, S. Z. et al. Accelerating industrial-level NO_3^- electroreduction to ammonia on Cu grain boundary sites via heteroatom doping strategy. *Small* **2023**, *19*, 2302295.

[53] Lu, Q.; Jiao, F. Electrochemical CO_2 reduction: Electrocatalyst, reaction mechanism, and process engineering. *Nano Energy* **2016**, *29*, 439–456.

[54] Zhou, J. W.; Xu, Z. H.; Cui, K.; Yin, J. A.; Chen, H. C.; Wang, Y. H.; Liu, F.; Wang, T. S.; Hao, F. K.; Xiong, Y. C. et al. Theory-guided design of unconventional phase metal heteronanostructures for higher-rate stable Li-CO_2 and Li-air batteries. *Angew. Chem., Int. Ed.* **2025**, *64*, e202416947.

[55] Ma, Y. B.; Sun, M. Z.; Xu, H. M.; Zhang, Q. H.; Lv, J.; Guo, W. H.; Hao, F. K.; Cui, W. T.; Wang, Y. H.; Yin, J. W.; Wen, H. Y. et al. Site-selective growth of fcc-2H-fcc copper on unconventional phase metal nanomaterials for highly efficient tandem CO_2 electroreduction. *Adv. Mater.* **2024**, *36*, 2402979.

[56] Ma, Y. B.; Yu, J. L.; Sun, M. Z.; Chen, B.; Zhou, X. C.; Ye, C. L.; Guan, Z. Q.; Guo, W. H.; Wang, G.; Lu, S. Y. et al. Confined growth of silver-copper Janus nanostructures with {100} facets for highly selective tandem electrocatalytic carbon dioxide reduction. *Adv. Mater.* **2022**, *34*, 2110607.

[57] Wang, X. D.; Hu, Q.; Li, G. D.; Yang, H. P.; He, C. X. Recent advances and perspectives of electrochemical CO_2 reduction toward C_{2+} products on Cu-based catalysts. *Electrochem. Energy Rev.* **2022**, *5*, 28.

[58] Nitopi, S.; Bertheussen, E.; Scott, S. B.; Liu, X. Y.; Engstfeld, A. K.; Horch, S.; Seger, B.; Stephens, I. E. L.; Chan, K.; Hahn, C. et al. Progress and perspectives of electrochemical CO_2 reduction on copper in aqueous electrolyte. *Chem. Rev.* **2019**, *119*, 7610–7672.

[59] Bi, X. Z.; Zhao, Y. Z.; Yan, Y. F.; Wang, H. Z.; Wu, M. B. Grain boundaries assisting the generation of abundant Cu^+ for highly selective electroreduction of CO_2 to ethanol. *Green Chem.* **2024**, *26*, 5356–5364.

[60] Wang, J.; Cheng, C.; Huang, B. L.; Cao, J. L.; Li, L. G.; Shao, Q.; Zhang, L.; Huang, X. Q. Grain-boundary-engineered La_2CuO_4 perovskite nanobamboos for efficient CO_2 reduction reaction. *Nano Lett.* **2021**, *21*, 980–987.

[61] Zhou, Y. N.; Ma, Y.; Shi, Z. N.; Zhou, J. C.; Dong, B.; Li, M. X.; Wang, F. G.; Liu, B.; Yu, J. F.; Chai, Y. M. Boosting oxygen evolution by nickel nitrate hydroxide with abundant grain boundaries via segregated high-valence molybdenum. *J. Colloid Interface Sci.* **2022**, *613*, 224–233.

[62] Sun, H. N.; Xu, X. M.; Kim, H.; Shao, Z. P.; Jung, W. Advanced electrocatalysts with unusual active sites for electrochemical water splitting. *InfoMat* **2024**, *6*, e12494.

[63] Xie, X. H.; Du, L.; Yan, L. T.; Park, S.; Qiu, Y.; Sokolowski, J.; Wang, W.; Shao, Y. Y. Oxygen evolution reaction in alkaline environment: Material challenges and solutions. *Adv. Funct. Mater.* **2022**, *32*, 2110036.

[64] Dong, Y.; Yang, J. T.; Liu, Y. J.; Wang, Y.; Dong, Z.; Cui, M. L.; Li,

M. X.; Yuan, X. L.; Zhang, X.; Dai, X. P. D Fe-doped NiO nanosheets with grain boundary defects for the advanced oxygen evolution reaction. *Dalton Trans.* **2020**, *49*, 6355–6362.

[65] Wang, L.; Qin, T.; Wang, J. J.; Wang, J. Y.; Zhang, J.; Cong, Y.; Li, X. K.; Li, Y. J. Grain boundary engineering of Co_3O_4 nanomeshes for efficient electrochemical oxygen evolution. *Nanotechnology* **2020**, *31*, 455401.

[66] Du, J.; Zhang, H.; Hu, W.; Li, Z. L.; Gao, W. S.; Wang, X. M.; Li, C. Grain boundary effects of hierarchical Ni-Fe (oxy)hydroxide nanosheets in water oxidation. *Small* **2023**, *19*, 2304245.

[67] Hou, X. H.; Liu, H. B.; Zhang, Q. C.; Fang, T. T.; Sun, M. H.; Peng, W. C.; Li, Y.; Zhang, F. B.; Fan, X. B. Grain-boundary-rich layered double hydroxides via a boron-assisted strategy for the oxygen evolution reaction. *Chem. Commun.* **2022**, *58*, 5646–5649.

[68] Wang, J. Q.; Xi, C.; Wang, M.; Shang, L.; Mao, J.; Dong, C. K.; Liu, H.; Kulinich, S. A.; Du, X. W. Laser-generated grain boundaries in ruthenium nanoparticles for boosting oxygen evolution reaction. *ACS Catal.* **2020**, *10*, 12575–12581.

[69] Zhao, X. H.; Li, Z. J.; Jang, H.; Wei, X. Q.; Wang, L.; Kim, M. G.; Cho, J.; Liu, X. E.; Qin, Q. D ruthenium-chromium oxide with rich grain boundaries boosts acidic oxygen evolution reaction kinetics. *Small* **2024**, *20*, 2311172.

[70] Zhao, Y. G.; Adiyeri Saseendran, D. P.; Huang, C.; Triana, C. A.; Marks, W. R.; Chen, H.; Zhao, H.; Patzke, G. R. Oxygen evolution/reduction reaction catalysts: From *in situ* monitoring and reaction mechanisms to rational design. *Chem. Rev.* **2023**, *123*, 6257–6358.

[71] Liu, X. J.; Yin, X.; Sun, Y. D.; Yu, F. J.; Gao, X. W.; Fu, L. J.; Wu, Y. P.; Chen, Y. H. Interlaced Pd-Ag nanowires rich in grain boundary defects for boosting oxygen reduction electrocatalysis. *Nanoscale* **2020**, *12*, 5368–5373.

[72] Wang, J.; Zhang, A.; Niu, W. X.; Liu, G. G.; Zhou, X. C.; Wang, L. X.; Liu, X. Z.; Li, L. J.; Li, Z. J.; Zhai, L. et al. 2H-Au nanosheet-templated growth of PdFe for electrocatalytic methanol oxidation. *Adv. Funct. Mater.* **2025**, *35*, 2405073.

[73] Wang, J.; Liu, G. G.; Yun, Q. B.; Zhou, X. C.; Liu, X. Z.; Chen, Y.; Cheng, H. F.; Ge, Y. Y.; Huang, J. T.; Hu, Z. N. et al. Epitaxial growth of unconventional 4H-Pd based alloy nanostructures on 4H-Au nanoribbons towards highly efficient electrocatalytic methanol oxidation. *Acta Phys.—Chim. Sin.* **2023**, *39*, 2305034.

[74] Wang, J.; Zhang, J.; Liu, G. G.; Ling, C. Y.; Chen, B.; Huang, J. T.; Liu, X. Z.; Li, B.; Wang, A. L.; Hu, Z. N. et al. Crystal phase-controlled growth of PtCu and PtCo alloys on 4H Au nanoribbons for electrocatalytic ethanol oxidation reaction. *Nano Res.* **2020**, *13*, 1970–1975.

[75] Wang, Z. N.; Huo, S. H.; Zhou, P. X. Rich-grain-boundary PtRuNi with network structure as efficient catalysts for methanol oxidation reaction. *Int. J. Electrochem. Sci.* **2019**, *14*, 10576–10581.

[76] Zhang, C.; Huang, H. J.; Gu, J. H.; Du, Z. G.; Li, B.; Li, S. M.; Yang, S. B. Fast Cryomediated dynamic equilibrium hydrolysates towards grain boundary-enriched platinum scaffolds for efficient methanol oxidation. *Research* **2019**, *2019*, 8174314.

[77] Yang, C. Z.; Jiang, Q. G.; Huang, H. J.; He, H. Y.; Yang, L.; Li, W. H. Polyelectrolyte-induced stereoassembly of grain boundary-enriched platinum nanoworms on $Ti_3C_2T_x$ MXene nanosheets for efficient methanol oxidation. *ACS Appl. Mater. Interfaces* **2020**, *12*, 23822–23830.

[78] Huang, H. J.; Wei, Y. J.; Yang, Y.; Yan, M. M.; He, H. Y.; Jiang, Q. G.; Yang, X. F.; Zhu, J. X. Controllable synthesis of grain boundary-enriched Pt nanoworms decorated on graphitic carbon nanosheets for ultrahigh methanol oxidation catalytic activity. *J. Energy Chem.* **2021**, *57*, 601–609.

[79] Meng, W.; He, H. Y.; Yang, L.; Jiang, Q. G.; Yuliarto, B.; Yamauchi, Y.; Xu, X. T.; Huang, H. J. 1D-2D hybridization: Nanoarchitectonics for grain boundary-rich platinum nanowires coupled with MXene nanosheets as efficient methanol oxidation electrocatalysts. *Chem. Eng. J.* **2022**, *450*, 137932.

[80] Yang, H.; Xie, J.; Liu, Y. Y.; Dong, Q. Z. Rational design of PdBi nanochains with grain boundaries for enhanced ethanol oxidation reaction. *Int. J. Hydrogen Energy* **2022**, *47*, 14859–14868.

[81] Wang, T. Z.; Cao, X. J.; Jiao, L. F. Progress in hydrogen production coupled with electrochemical oxidation of small molecules. *Angew. Chem.* **2022**, *134*, e202213328.

[82] Sun, H. N.; Xu, X. M.; Fei, L. S.; Zhou, W.; Shao, Z. P. Electrochemical oxidation of small molecules for energy-saving hydrogen production. *Adv. Energy Mater.* **2024**, *14*, 2401242.

[83] Geng, X.; Li, S. W.; Heo, J.; Peng, Y.; Hu, W. H.; Liu, Y. C.; Huang, J. E.; Ren, Y.; Li, D. S.; Zhang, L. et al. Grain-boundary-rich noble metal nanoparticle assemblies: Synthesis, characterization, and reactivity. *Adv. Funct. Mater.* **2022**, *32*, 2204169.

[84] He, T. W.; Zhang, C. M.; Du, A. J. Single-atom supported on graphene grain boundary as an efficient electrocatalyst for hydrogen evolution reaction. *Chem. Eng. Sci.* **2019**, *194*, 58–63.

[85] Wang, S. H.; Huang, B. B.; Dai, Y.; Wei, W. Origin of the enhanced hydrogen evolution reaction activity of grain boundaries in MoS_2 monolayers. *J. Phys. Chem. C* **2022**, *126*, 6215–6222.

[86] Zhao, Y.; Chen, Y. Q.; Ou, P. F.; Song, J. Basal plane activation via grain boundaries in monolayer MoS_2 for carbon dioxide reduction. *ACS Catal.* **2023**, *13*, 12941–12951.

[87] Gao, L. K.; Cui, X.; Sewell, C. D.; Li, J.; Lin, Z. Q. Recent advances in activating surface reconstruction for the high-efficiency oxygen evolution reaction. *Chem. Soc. Rev.* **2021**, *50*, 8428–8469.

[88] Ma, X.; Ma, C. Q.; Xia, J.; Han, S. M.; Zhang, H. F.; He, C. H.; Feng, F. K.; Lin, G.; Cao, W. B.; Meng, X. M. et al. Heterophase intermetallic compounds for electrocatalytic hydrogen production at industrial-scale current densities. *J. Am. Chem. Soc.* **2024**, *146*, 20594–20603.

This is an open access article under the terms of the Creative Commons Attribution 4.0 International License (CC BY 4.0, https://creativecommons.org/licenses/by/4.0/).

© The Author(s) 2026. Published by Tsinghua University Press.